

OMAE2013- 10625

FATIGUE ANALYSIS OF FREE SPANNING PIPELINES SUBJECTED TO VORTEX INDUCED VIBRATIONS

F. Van den Abeele
Fugro GeoConsulting Belgium
Brussels, Belgium

F. Boël
Fugro GeoConsulting Belgium
Brussels, Belgium

M. Hill
Shell Exploration & Production
Houston, Texas, US

ABSTRACT

Vortex induced vibration is a major cause of fatigue failure in submarine oil and gas pipelines and steel catenary risers. Even moderate currents can induce vortex shedding, alternately at the top and bottom of the pipeline, at a rate determined by the flow velocity. Each time a vortex sheds, a force is generated in both the in-line and cross-flow direction, causing an oscillatory multi-mode vibration. This vortex induced vibration can give rise to fatigue damage of submarine pipeline spans, especially in the vicinity of the girth welds.

In this paper, an integrated numerical framework is presented to predict and identify free spans that may be vulnerable to fatigue damage caused by vortex induced vibrations (VIV). An elegant and efficient algorithm is introduced to simulate offshore pipeline installation on an uneven seabed. Once the laydown simulation has been completed, the free spans can be automatically detected. When the fatigue screening for both in-line and cross-flow VIV indicates that a particular span may be prone to vortex induced vibrations, a detailed fatigue analysis is required.

Amplitude response models are constructed to predict the maximum steady state VIV amplitudes for a given pipeline configuration (mechanical properties) and sea state (hydrodynamic parameters). The vibration amplitudes are translated into corresponding stress ranges, which then provide an input for the fatigue analysis. A case study from the offshore industry is presented, and sensitivity analyses are performed to study the influence of the seabed conditions, where special emphasis is devoted on the selection of pipe soil interaction parameters.

VORTEX INDUCED VIBRATIONS FOR SUBSEA PIPES

The on bottom stability of offshore pipelines is governed by the Morison's equations [1-2], a semi-empirical set of equations relating the pipeline diameter to the hydrodynamic forces (lift, drag and inertia). In addition to these forces, a turbulent von Karman vortex street can appear in the wake of a subsea pipeline for certain combinations of dimensions and flow velocities. Each time a vortex sheds, a force is generated both in the in-line and cross-flow direction, causing an oscillatory multi-mode vibration. When the vortex shedding frequency is close to the natural frequency of the structure, resonance or 'lock-in' could occur, which may jeopardize the integrity of the structure. Figure 1 shows a von Karman vortex street in the wake of a subsea pipeline at the onset of turbulence.

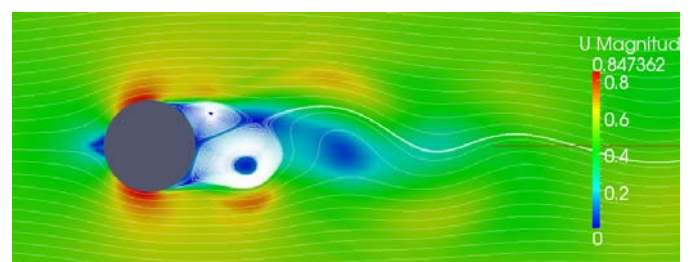


Figure 1: Von Karman street at the onset of turbulence

Due to the alternating vortex wake, the oscillations in lift force $L(t)$ occur at the vortex shedding frequency f_s , and oscillations in drag force $D(t)$ occur at twice this frequency. Figure 5 shows the evolution of the fluctuating lift and drag forces exerted on an offshore pipeline span.

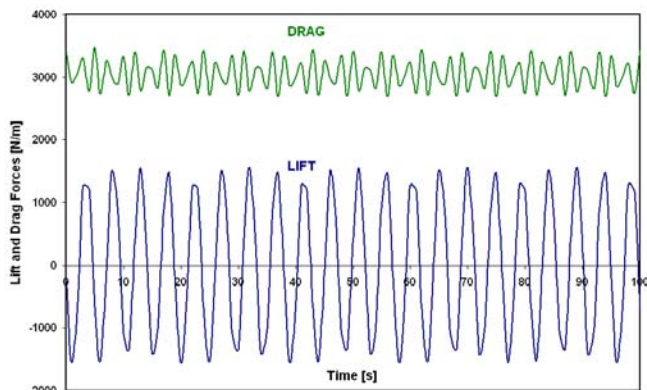


Figure 2: Lift and drag forces on an offshore pipeline span

The oscillating signals reflect a fully developed turbulent wake. Note that the average lift force is zero, while the average drag force is a measure for the resistance against fluid flow. On Figure 3, the Fast Fourier Transform (FFT) of the lift and drag forces is shown, to reveal the frequency content of the signals. Clearly, the dominant frequency of the drag force is twice the lift frequency.

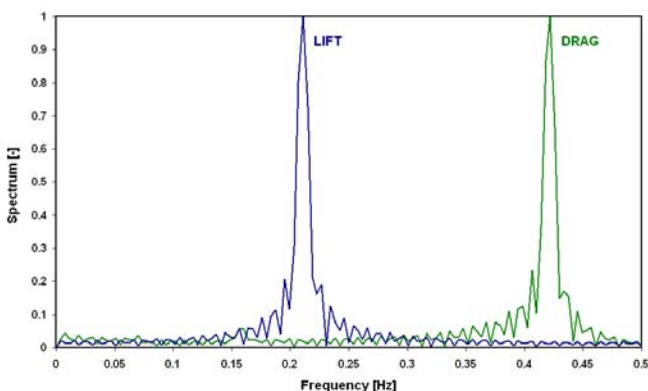


Figure 3: Frequency spectrum of lift and drag forces

Like shown on Figure 4, these in-line and cross-flow oscillations can give rise to an '8'-shaped motion of the pipeline span, which is detrimental to its fatigue life. A comprehensive overview on vortex induced vibrations is given in [3, 4], and a more recent review on VIV experiments and simulations for offshore pipelines can be found in e.g. [5-7].

In this paper, an integrated numerical framework is presented to predict and identify free spans that may be vulnerable to vortex induced vibrations (VIV):

- First, an elegant and efficient algorithm is introduced to simulate offshore pipeline installation on an uneven seabed. Once the laydown simulation has been completed, the free spans can be automatically detected.

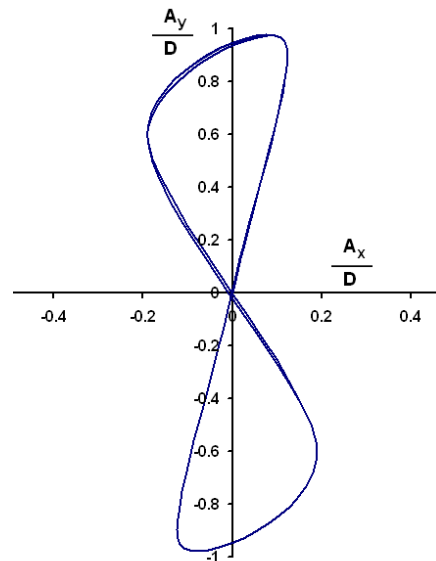


Figure 4: Path of a pipeline subjected to VIV

- Then, a case study from the offshore pipeline industry is presented to reveal the influence on the pipe soil interaction parameters on the span prediction.
- At the end of this paper, a remaining lifetime assessment is presented for the identified critical spans. Indeed, when the fatigue screening for both in-line and cross-flow VIV indicates that a particular span may be prone to vortex induced vibrations, DNV-RP-F105 [8] recommends to perform a full fatigue analysis based on an amplitude response model [8, 9].

SIMULATING PIPE LAYDOWN AND INSTALLATION

Offshore pipeline installation is performed from a lay barge, typically in S-lay configuration. For smaller diameters, pipeline reeling can be the most cost efficient solution, whereas J-lay is the only feasible approach in (ultra) deep water. Depending on the installation method, the pipeline is subjected to different load patterns during installation, including hydrostatic pressure, lay tension and bending on the stinger and in the sagbend. A comprehensive overview on the mechanics of installation design can be found in [10].

The simulation of the pipelaying process is one of the most challenging tasks once the optimum route has been selected. Implementing pipeline installation in a general purpose finite element package can be a time consuming and tedious job, in particular when importing vast amounts of seabed data. Most often, advanced scripting techniques are required to define the seabed profile, select the optimum pipeline route and simulate the laydown process. In addition, the available constitutive models for pipe-soil interaction may not comply with industry standards.

In this paper, the SAGE Profile software suite [11, 12] is used to simulate pipelaying on an uneven seabed, and evaluating the susceptibility of free spans to vortex induced vibrations. This finite element analysis software has been tailored to assist the pipeline engineer during offshore pipeline design. Using a transient dynamic explicit solver, it can accurately mimic the actual pipeline installation process.

The pipe is simulated by discretising the entire pipeline into section of finite length. These sections are represented by beam elements with 12 degrees of freedom (DOF), bounded at either side by nodes. The distributed mass of the pipe is lumped at these nodes. The finite element kernel uses an explicit integration algorithm, which computes the dynamic motion of the pipe and is therefore ideally suited to simulate the pipe laying process.

During this pipeline installation process, new pipe elements are continuously created and the pipe is laid along the target path defined on the seabed. The residual lay tension T at the seabed is used as an input and the unstressed length L_0 of the last element is updated such that the axial force corresponds to the applied lay tension:

$$\frac{L - L_0}{L_0} EA - F_p = T \quad (03)$$

with L the original element length,

$$A = \frac{\pi}{4} (D_o^2 - D_i^2) \quad (04)$$

the cross sectional area of a circular pipe with inner diameter D_i and outer diameter D_o , and

$$F_p = (1 - 2\nu)(p_o A_o - p_i A_i) \quad (05)$$

the pressure induced axial force component, accounting for both the internal pressure p_i and the (hydrostatic) external pressure p_o . As a result, both empty and water filled installation can be simulated. In (03), ν is the Poisson's coefficient of the pipeline steel, where A_i and A_o are the surface areas of the interior and exterior of the pipe respectively. When the growing element becomes longer than twice the initial length, the element is split in two new elements. An additional node is placed along the last element such that the newly formed element obtains the original unstressed length.

This algorithm accurately reflects the continuous supply of welded pipe joints from a moving lay barge. The gravity, applied during the pipelay simulation, will force the newly created pipe elements into place. Figure 5 shows the typical catenary shape during pipeline installation.

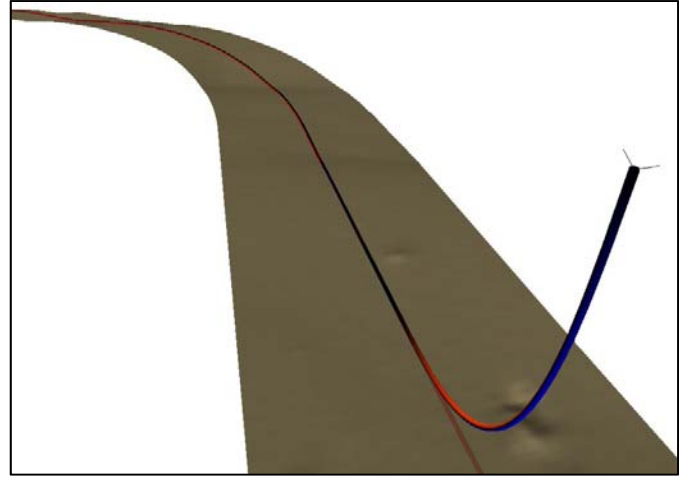


Figure 5: Pipeline catenary shape during S-lay installation

For long pipelines and significant water depths, simulating the entire laydown process (from the barge down to the seabed) tends to be time consuming and is computationally expensive. The sophisticated architecture of the solver used for this analysis allows for a significant reduction in the resources required to simulate pipeline laydown. By default, the lay barge and most of the free hanging pipe is replaced by a single feeding point in the water column moving close to the seabed, like shown on Figure 6.

This feeding point acts as a submarine lay barge, generating new pipe joints as it moves forward. The lay tension is now applied at the feeding point, generating a residual on bottom tension in the laid pipe section.

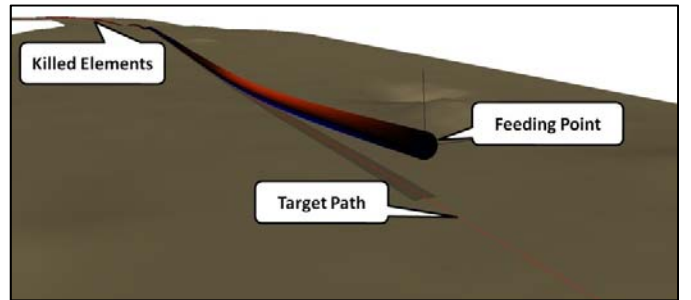


Figure 6: Definition of feeding point and target path

Assuming a catenary shape [10], the lay tension at the feeding point can be expressed in terms of the submerged weight per unit length w_s

$$T = \frac{h w_s}{\tan^2 \theta} \left(1 + \sqrt{1 + \tan^2 \theta} \right) \quad (07)$$

where θ is the angle between the pipe and the target path, and h is the height of the feeding point above the seabed. Replacing the lay barge with a feeding point close to the seabed allows for a significant reduction in calculation time, without losing accuracy. Given the inherent complexity of pipeline laying, an accurate and robust steering mechanism of the feeding point is of paramount importance. The steering mechanism is governed by a Proportional-Integrating-Differentiating (PID) controller, providing a smooth movement of the feeding point and ensuring that the pipeline is installed on the pre-defined target path (shown in red on Figure 6).

In addition to the concept of a feeding point, an efficient element killing procedure has been implemented to control the computational effort during pipeline laydown. Indeed, it would be too expensive to simulate the entire length of the pipe from its starting point up to the feeding point. In order to reduce the required calculation time, elements that are already lying on the seabed and are no longer moving will be removed from the simulation. If the magnitude of the velocity vector for a node is lower than a pre-defined threshold, the associated element has little or no contribution to the simulation results and can be killed without losing accuracy. On Figure 6, the elements that have been killed are shown as well.

IDENTIFICATION OF FREE SPANNING PIPELINES

Accurate prediction of free spans (location, length and height) is an important prerequisite in offshore pipeline design. Indeed, free span lengths should be maintained within an allowable range [07], which is determined during the design phase. Pipelines installed on a very rough seabed can cause a high number of free spans that can be difficult to rectify. A judicious assessment of free spans can dramatically reduce the costs associated with seabed intervention (trenching, rock dumping and span supports).



Figure 7: Free spanning pipeline on an uneven seabed

Figure 7 demonstrates that finite element methods are capable of simulating pipeline installation on an uneven seabed, and subsequently detecting free spans.

In this paper, a case study from the offshore industry is presented to demonstrate the added value of numerical simulations to predict fatigue damage in free spanning pipes. An X70 flowline with an outer diameter $D_o = 10\text{-}3/4$ " (273.05 mm) and a wall thickness $t_s = 7/8$ " (22.225 mm) is installed in the Gulf of Mexico in water depths exceeding 2400 meters. The irregular seafloor topography, shown on Figure 8, indicates that this pipeline may be prone to free spans and hence vulnerable to vortex induced vibrations.

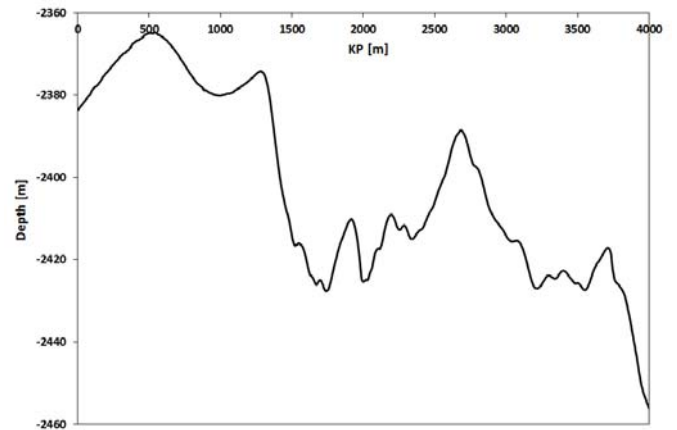


Figure 8: Seabed roughness along the pipeline route

The pipe is coated with a Fusion Bonded Epoxy (FBE) coating and a Glass Syntactic Polyurethane (GSPU) coating with mechanical properties summarized in Table 1.

Table 1: Mechanical properties of the coating layers

Coating	Thickness ["]	Density [kg/m ³]	Water Absorption [%]
FBE	0.018	1440	0
GSPU	3	833	5

The soil conditions along the route consist mainly of very soft clay, typical for deepwater soils encountered in the Gulf of Mexico. For the finite element simulations, presented here, a submerged unit weight of $\gamma_s = 7.5 \text{ kN/m}^3$ is taken. The green dots on Figure 9 represent field measurements of the undrained shear strength S_u as a function of depth. In this paper at hand, we have used a bilinear approximation

$$S_u(z) = \begin{cases} S_u(0) + k_1 z & 0 \leq z \leq z^* \\ S_u(z^*) + k_2 z & z > z^* \end{cases} \quad (08)$$

like indicated by the blue lines on Figure 9. For the data set presented in Figure 9, values for ground surface shear strength $S_u(0) = 0.39 \text{ kPa}$ and strength increase rate $k_1 = 12.27 \text{ kPa/m}$ and $k_2 = 2.5 \text{ kPa/m}$ were obtained.

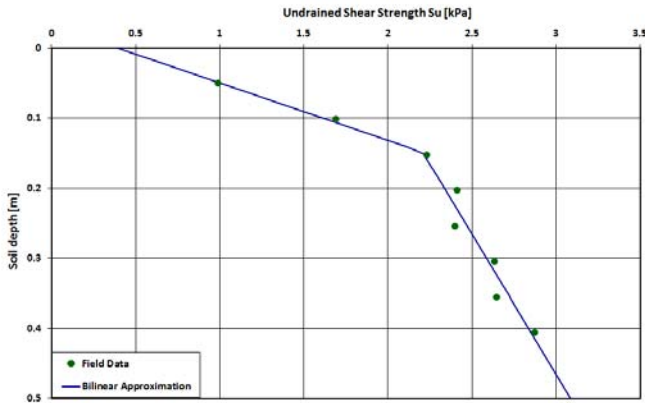


Figure 9: Undrained shear strength profile

This bilinear shear strength profile is converted into a non-linear soil spring using the power-relationship

$$\frac{F}{D} = S_u(z) \cdot a \cdot \left(\frac{z}{D}\right)^b \quad (08)$$

proposed by Aubeny [13] to relate the dimensionless bearing resistance F/D with the normalized pipeline embedment z/D . The catenary shape of the suspended pipeline during laying (schematically shown on Figure 5) has been taken into account to accurately capture the pipe embedment at the touchdown point, and an enhanced soil model [12] is used to reflect the elastoplastic soil behavior. The lateral and axial soil springs are defined by a friction factor and a limiting soil resistance.

Simulation of the pipe laying process has been performed with an element length of 1 meter, and assuming a residual bottom tension $T = 100$ kN. After the pipelay simulation has been completed, the software automatically detects the spans over the entire pipeline route, and plots the span location, length and height in comprehensive and easy-to-read design charts, like shown on Figure 11.

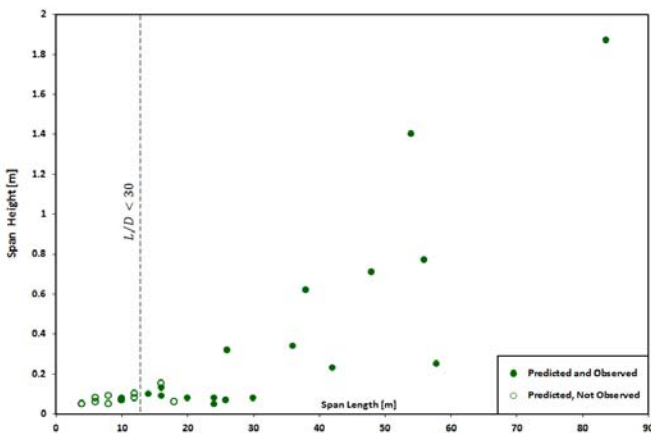


Figure 10: Comparison of observed and predicted spans

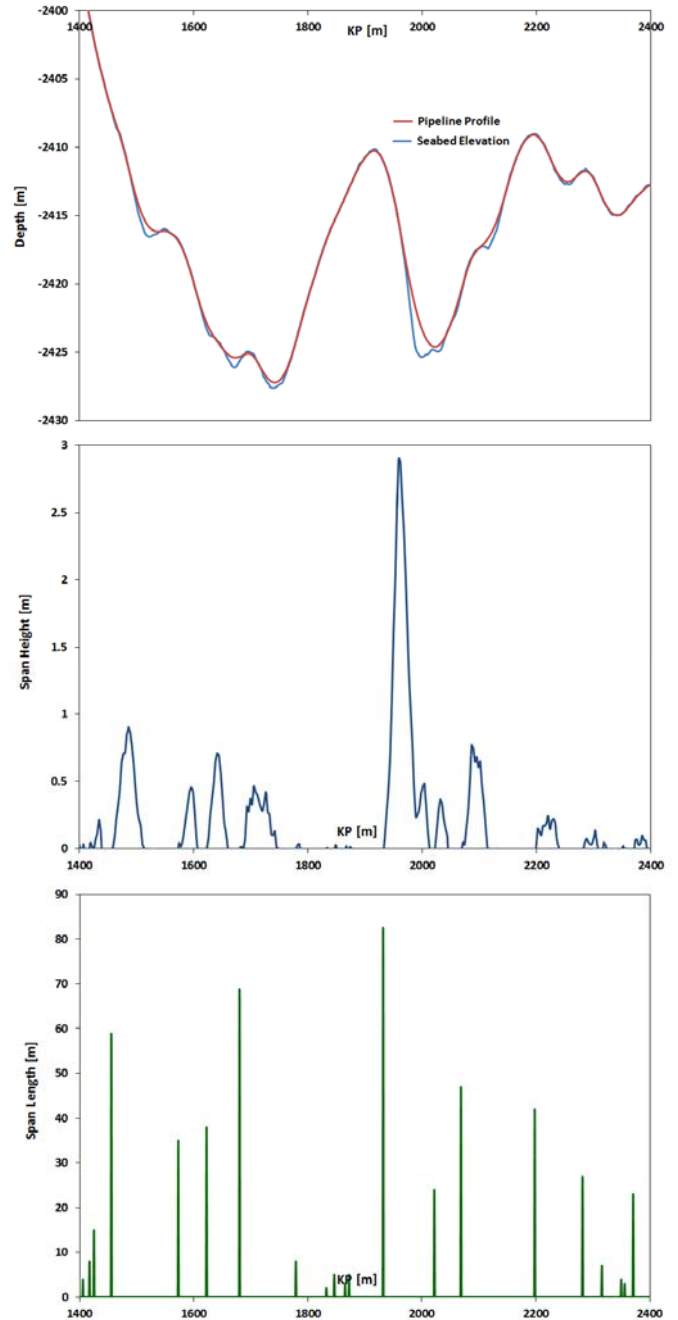


Figure 11: Overview of span location, height and length

On Figure 10, the observed spans (from an as-laid survey) are compared to the spans predicted by the simulations. A span is judged to be ‘predicted’ (solid green dots) when the KP range of the observed and simulated spans overlap for more than 50%. Although detailed analysis revealed that the length and height for some simulated spans was slightly underestimated, the predictions correspond fairly well to the observed spans.

The finite element tool has identified a number of low rising spans (with a gap between the pipe surface and the seabed lower than 0.2 meters) that have not been observed during the as-laid survey. This may be attributed to the resolution of the survey equipment, or to numerical artifacts (especially for short, low rising spans). Most of the predicted spans that have not been observed have a normalized span length $L/D_{tot} < 30$, with D_{tot} the total pipe diameter (including all coatings). For such spans, insignificant dynamic response from environmental loads is expected [8]. Hence, they are unlikely to experience vortex induced vibrations.

Sensitivity analyses were performed to investigate the influence of element length, soil conditions and lay tension on the ability to predict free spanning pipes. These analyses indicate that

- Reducing the element length enhances the accuracy of the simulated spans. The lower bound for the element length is governed by the seabed resolution.
- The suspended catenary has to be taken into account to capture the actual pipeline embedment at the touch-down point.
- The predicted span length and height are sensitive to the constitutive soil model. An elastic soil model tends to over-estimate the span length. Hence, an elasto-plastic soil model with bearing resistance based on a bilinear depth profile for the undrained shear strength is recommended.
- The applied residual lay tension has a pronounced influence on the span predictions. The simulated span lengths increase with increasing lay tension. This is in line with the observations reported in [14] on influence of the effective axial force on free spanning pipes.

FATIGUE ANALYSIS FOR SPANS SUBJECTED TO VIV

Once the laydown simulation is performed, the solver automatically detects the spans over the entire pipeline route, like shown on Figure 11. The plots of seabed roughness, pipeline profile, span height and span length clearly indicate the presence of a long free span starting at KP ~ 1940m. This free span, with a length of 82 m and a maximum gap of 1.9 m, is shown on Figure 12, where the color code reflects the span gap.

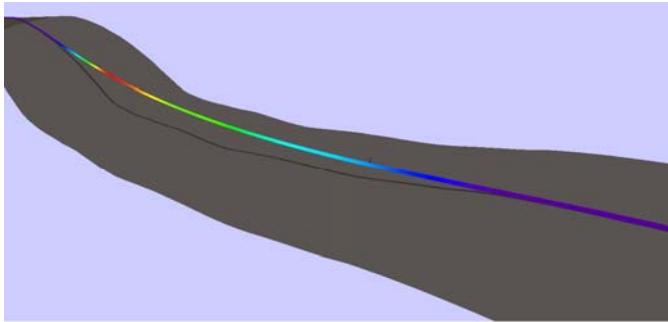


Figure 12: Long free spanning pipeline vulnerable to VIV

Next, we perform a DNV-RP-F105 [8] span check to evaluate whether such free spans are susceptible to fatigue damage induced by VIV. For each detected span, we calculate the associated reduced velocity

$$V_R = \frac{U_c + U_w}{f_0 D_{tot}} \quad (9)$$

where U_c is the mean current velocity (normal to the pipe), U_w the significant wave-induced flow velocity, and f_0 an approximation for the lowest natural frequency given by

$$f_0 \approx \sqrt{1 + CSF} \sqrt{\frac{EI}{m_e L_e^4} \left[1 + \frac{F_e}{P_{cr}} + C_3 \left(\frac{\delta}{D_o} \right)^2 \right]} \quad (10)$$

with CSF the stiffening effect of the concrete coating, L_e the effective span length [10], m_e the effective mass, F_e the effective axial force, δ the static deflection and C_3 the end boundary coefficient. The moment of inertia for the hollow circular pipe is given by

$$I = \frac{\pi}{64} (D_o^2 - D_i^2) \quad (11)$$

and the critical buckling load can be calculated as

$$P_{cr} = (1 + SCF) C_2 \left(\frac{\pi}{L_e} \right)^2 EI \quad (12)$$

where C_2 is an end boundary coefficient as well. In addition to the reduced velocity (9), we calculate the stability parameter

$$K_s = 4 \pi \frac{m_e \zeta_T}{\rho_w D_o^2} \quad (13)$$

for each span, where ζ_T is the total modal damping ratio, comprising structural damping, hydrodynamic damping and soil damping.

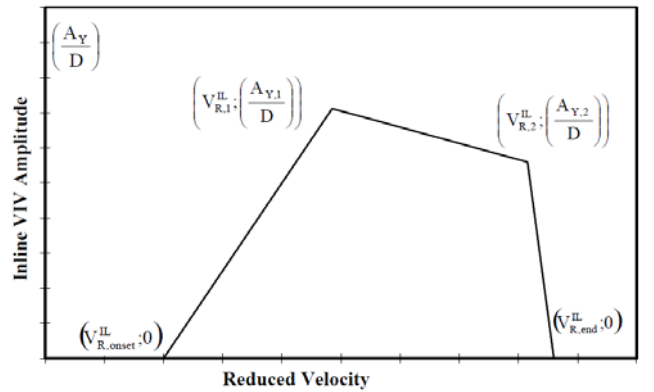


Figure 13: Response model for in-line VIV motion

Based on the values of the reduced velocity (9) and the corresponding stability parameter (13), the in-line vibration amplitude can be estimated based on the response model shown in Figure 13, and presented in the Appendix.

For the (ultra)deep water pipeline, presented in this paper, the contribution of wave induced velocities is neglected, i.e. we assume $U_w \approx 0$ m/s. The current velocity is typically specified as a Weibull probability density function [15], which can be estimated from the 1, 10 and 100 y return period. Since no detailed metocean data was available, and given the magnitude of the water depth (exceeding 2400 meter), we have used a uniform current velocity distribution of $U_c \approx 0.1$ m/s in this paper. Under these hydrodynamic conditions, the reduced velocity for the long span, shown in Figure 12, exceeds the threshold for the onset of in-line VIV:

$$V_R = \frac{U_c + U_w}{f_1 D_{tot}} = 1.18 > 0.909 = V_{R,onset}^{II} \quad (14)$$

This allows calculating the maximum allowable span length that satisfies $V_R < V_{R,onset}^{II}$ as $L_{max} = 65.8$ meter. The in-line vibration amplitude can be determined from the response model (shown on Figure 13) as the value of that corresponds with the design value of the reduced velocity

$$V_{Rd} = V_R \gamma_f \quad (15)$$

with γ_f the safety factor for the natural frequency, which depends on the safety class and whether the span is (very) well defined or not [8].

The dimensionless vibration amplitude A_y/D_{tot} can then be translated into a stress range

$$S_{IL} = 2 A_{IL} \left(\frac{A_y}{D_{tot}} \right) \psi_\alpha^{II} \gamma_s \quad (16)$$

with γ_s a safety factor, ψ_α^{II} the reduction factor for the current flow ratio

$$\alpha = \frac{U_c}{U_c + U_w} \quad (17)$$

and A_{IL} the unit stress amplitude, i.e. the stress due to unit diameter in-line mode shape deflection. According to DNV-RP-F105 [8], the unit stress amplitude may be approximated as

$$A_{IL} = C_4 (1 + CSF) \frac{D_{tot} (D_o - t_s) E_s}{L_{eff}^2} \quad (18)$$

with C_4 the mid-span boundary condition coefficient and E_s the stiffness of steel.

The number of cycles to failure N_{IL} at a stress range S_{IL} is defined by an SN-curve of the form

$$S = \begin{cases} \bar{a}_1 \cdot S^{-m_1} & S > S_{sw} \\ \bar{a}_2 \cdot S^{-m_2} & S \leq S_{sw} \end{cases} \quad (19)$$

where $\{m_1, m_2\}$ are fatigue exponents (i.e. the inverse slope of the bi-linear SN curve), $\{\bar{a}_1, \bar{a}_2\}$ are characteristic fatigue strength constants, and

$$S_{sw} = 10^{\left(\frac{\log \bar{a}_1 - \log N_{sw}}{m_1} \right)} \quad (20)$$

is the stress at the intersection of the two SN-curves, with the number of cycles for which the change in slope appears. Typically, $\log N_{sw}$ is either 6 or 7. The SN-curves may be determined from dedicated laboratory test data, accepted fracture mechanics theory, or the values recommended in [16].

For fatigue calculations, the pipeline design engineer can either define his own SN curve, or select the SN-curves $\{F, F_1, F_2, F_3\}$ from DNV-RP-C203. The latter curves have a different shape for free corrosion (only one slope) or when cathodic protection is present (two-slope curve). For instance, the SN curves in seawater when cathodic protection is present are shown on Figure 14. The change in slope occurs at $N_{sw} = 10^6$. For the fatigue analysis, presented here, we have used the F_3 SN-curve from [16], assuming cathodic protection is present.

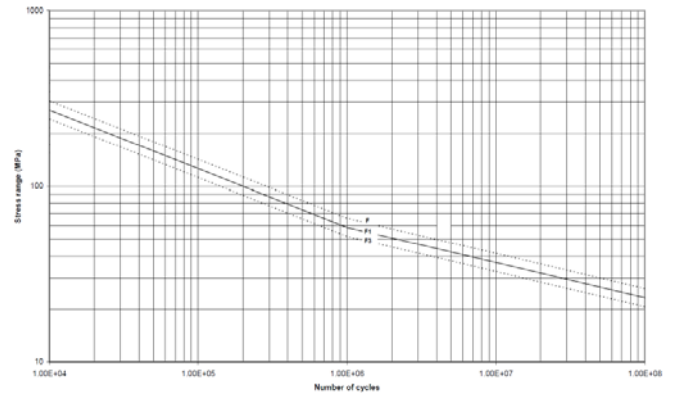


Figure 14: SN curves for cathodically protected pipelines

The marginal fatigue life capacity against in-line VIV in a single sea-state is calculated by integrating over the long-term distribution of the current velocity. As we assume a uniform current velocity distribution, the fatigue life calculation simplifies to

$$T_{IL}[y] = \frac{N_{IL}/f_0}{365 \cdot 24 \cdot 3600} \quad (21)$$

For the critical free span shown in Figure 12, this leads to a remaining fatigue life of 116 years, which is well above the design life of the flowline.

In addition to the in-line VIV assessment, we can also construct the response model for cross-flow VIV, based on the current flow ratio (17), and the Keulegan Carpenter number

$$KC = \frac{U_w}{f_w D_{tot}} \quad (22)$$

with U_w the significant wave-induced velocity, and f_w the corresponding frequency. Given the significant water depths, exceeding 2400 meters, fatigue analysis for both cross-flow VIV and cross-flow induced VIV can be omitted.

CONCLUSIONS

In this paper, an integrated numerical framework was presented to predict and identify free spans that may be vulnerable to fatigue damage caused by vortex induced vibrations (VIV). An elegant and efficient algorithm was introduced to simulate offshore pipeline installation on an uneven seabed. Once the laydown simulation has been completed, the free spans can be automatically detected.

When the fatigue screening for both in-line and cross-flow VIV indicates that a particular span may be prone to vortex induced vibrations, a detailed fatigue analysis is required. SAGE Profile offers a DNV-RP-F105 span check, which covers fatigue screening (in-line VIV, cross flow VIV and direct wave action) and more detailed fatigue analysis.

When free spans are prone to VIV, amplitude response models are constructed to predict the maximum steady state VIV amplitudes. The vibration amplitudes are translated into corresponding stress ranges, which then provide an input for the fatigue analysis.

A case study from the offshore industry was presented. For a deepwater pipeline in the Gulf of Mexico, the remaining fatigue capacity of a long slender span subjected to VIV was analyzed using this span check.

This powerful capability provides a quick and easy tool to evaluate the severity of free spans for a given pipeline route, and hence can save a tremendous amount of time and money associated with seabed rectification.

APPENDIX: RESPONSE MODEL FOR IN-LINE VIV

The in-line response of a pipeline span in current dominated conditions (like the one shown on Figure 12) is associated with either alternating or symmetric vortex shedding. Contributions from the first instability region and the second instability region are included in the response model proposed in [8]. This response model, schematically shown on Figure 13, can be constructed based on the design value of the stability parameter $K_{sd} = K_s/\gamma_k$, where γ_k is a safety factor.

The *onset* velocity $V_{R,onset}^{IL}$ is the value for the reduced velocity where in-line VIV starts to occur:

$$V_{R,onset}^{IL} = \begin{cases} \frac{1.0}{\gamma_{on}^{IL}} & \text{for } K_{sd} < 0.4 \\ 0.6 + K_{sd} & \text{for } 0.4 < K_{sd} < 1.6 \\ \frac{2.2}{\gamma_{on}^{IL}} & \text{for } K_{sd} > 1.6 \end{cases} \quad (23)$$

and the *end* velocity can be written as

$$V_{R,end}^{IL} = \begin{cases} 4.5 - 0.8 K_{sd} & \text{for } K_{sd} < 1.0 \\ 3.7 & \text{for } K_{sd} \geq 1.0 \end{cases} \quad (24)$$

The reduced velocities for the other two points indicated in Figure 13 are given by

$$V_{R,1}^{IL} = 10 \frac{A_{Y,1}}{D_{tot}} + V_{R,onset}^{IL} \quad (25)$$

$$V_{R,2}^{IL} = V_{R,end}^{IL} - 2 \frac{A_{Y,2}}{D_{tot}} \quad (26)$$

where $A_{Y,1}$ and $A_{Y,2}$ are the corresponding vibration amplitudes

$$\frac{A_{Y,1}}{D_{tot}} = \max \left[0.18 \left(1 - \frac{K_{sd}}{1.2} \right) R_1^{I\theta}; \frac{A_{Y,2}}{D_{tot}} \right] \quad (27)$$

and

$$\frac{A_{Y,2}}{D_{tot}} = 0.13 \left(1 - \frac{K_{sd}}{1.8} \right) R_2^{I\theta} \quad (28)$$

These amplitude values depend on the reduction factors $0 \leq R_1^{I\theta}(I_c, \theta_{rel}) \leq 1$ and $0 \leq R_2^{I\theta}(I_c, \theta_{rel}) \leq 1$ who account for the effect of the turbulence intensity I_c and the angle of attack (θ_{rel} , in radian) for the flow [8].

Also note that DNV-RP-F105 introduces an additional reduction function to account for reduced in-line VIV in wave dominated conditions:

$$\psi_{\alpha}^{IL} = \begin{cases} 0.0 & \text{for } \alpha < 0.5 \\ \frac{\alpha - 0.5}{0.3} & \text{for } 0.5 < \alpha < 0.8 \\ 1.0 & \text{for } \alpha > 0.8 \end{cases} \quad (29)$$

Thus, if $\alpha < 0.5$, in-line VIV may be ignored.

REFERENCES

- [1] Morison J.R., O'Brien M.P., Johnson J.W. and Schaaf S.A., The Forces Exerted by Surface Waves on Piles, *Journal of Petroleum Technology*, vol. 189, pp. 149-154 (1950)
- [2] Van den Abeele F. and Vande Voorde J., Stability of Offshore Pipelines in Close Proximity to the Seabed, *Proceedings of the 6th Pipeline Technology Conference*, Hannover, Germany (2011)
- [3] King R., A Review of Vortex Shedding Research and its Application, *Ocean Engineering*, vol. 4, pp. 141-172 (1977)
- [4] Sarpkaya T., Vortex Induced Vibrations: a Selective Review, *Journal of Applied Mechanics*, vol. 46(2), pp. 241-258 (1979)
- [5] Goswami I., Scanlan R.H. and Jones N.P., Vortex Induced Vibration of Circular Cylinders: Experimental Data and New Models, *Journal of Engineering Mechanics*, vol. 119 (11), pp. 2270-2302 (1993)
- [6] Gabbai R.D. and Benaroya H., An Overview of Modelling and Experiments of Vortex Induced Vibrations for Circular Cylinders, *Journal of Sound and Vibrations*, vol. 282, pp. 575-919 (2005)
- [7] Fortaleza R., Analysis of Phenomenological Models of Vortex Induced Vibrations, *Proceedings of the 30th ASME Conference on Ocean, Offshore and Arctic Engineering*, OMAE2011-49403 (2011)
- [8] Det Norske Veritas, Recommended Practice on Free Spanning Pipelines, DNV-RP-F105 (2006)
- [9] Fyrileiv O., Mork K., Chezhian M. and Nielsen F.G., Updated Free Span Procedure DNV-RP-F105: Ormen Lange Experience, *Journal of Pipeline Engineering*, Q2, pp. 81-94 (2006)
- [10] Bai Y. and Bai Q., Pipelines and Risers, Chapter 34: Installation Design, pp. 597-636 (2005)
- [11] Witgens J.F., Falepin H. and Stephan L., New Generation Pipeline Analysis Software, *Offshore Pipeline Technology*, OPT 2006
- [12] Van den Abeele F. and Denis R., Numerical Modelling and Analysis for Offshore Pipeline Design, Installation and Operation, *Journal of Pipeline Engineering*, Q4, pp. 273-286 (2011)
- [13] Aubeny C.P., Shi H. and Murf J.D., Collapse Loads for a Cylinder Embedded in Trench in Cohesive Soil, *International Journal of Geomechanics*, vol. 5(4), pp. 320-325 (2005)
- [14] Hagen O., Mork K.J., Nielsen F.G. and Soreide T., Evaluation of Free Spanning Design in a Risk Based Perspective, *Proceedings of the 22nd Conference on Offshore Mechanics and Arctic Engineering*, OMAE-37419 (2003)
- [15] Fyrileiv O., Aronsen K. and Mork K., DNV FatFree Verification Document, Report No. 2000-3283 (2010)
- [16] Det Norske Veritas, Recommended Practice on Fatigue Design of Offshore Steel Structures, DNV-RP-C203 (2010)